HIGH TECHNOLOGY LETTERS | Vol. 31 No. 1 | Mar. 2025 | pp. 95-104

doi:10.3772/j.issn.1006-6748.2025.01.010

Study on pressure buffer structure of continuous rotary electro-hydraulic servo motor①

WANG Xiaojing (王晓晶)②, PENG Ziqin, ZHANG Yuxuan
(Beijing Key Laboratory of Performance Guarantee on Urban Rail Transit Vehicle, Beijing University of Civil Engineering and Architecture, Beijing 102616, P. R. China)
(Beijing Engineering Research Center of Monitoring for Construction Safety, Beijing University of Civil Engineering and Architecture, Beijing 102616, P. R. China)

Abstract

The aim of the study is to investigate the impact of the buffer groove structure on the pressure of continuous rotation electro-hydraulic servo motor. The mathematical model of the motor valve plate with triangular groove and U-groove structure is established firstly, and the structure size of the two buffer grooves with better pressure drop effect is obtained by Matlab. Secondly, an established pressure gradient model is developed for the sealed canisters for electric motors using a combined groove structure. The bird swarm optimization algorithm is used to obtain the optimal dimensions for the combined depth and angle of the pressure groove. The flow field in the motor seal chamber is simulated and calculated by Fluent. This study compared the pressure field distributions in the motor's sealing chamber using triangular and combined groove structures. It investigated the combined groove's effect on the pressure impact during the commutation of a continuously rotating electro-hydraulic servo motor. It is found that the combined groove structure has a positive impact on reducing the pressure impact. The results indicate that the combined groove structure significantly enhances the efficiency of mitigating pressure shocks when the motor switches between high- and low-pressure chambers.

Key words: continuous rotating electro-hydraulic servo motor, pressure impact, combined groove, optimal design

0 Introduction

Electro-hydraulic servo motor has the characteristics of high precision, low rotational speed, fast frequency response and fast speed regulation. It has been employed in a diverse range of applications, including flight simulation turntables in the aerospace industry, drive components of computer numerical control (CNC) machine tools, hydraulic servo systems for ships, robot joints, automotive braking devices, and so forth[1-6]. However, the operation of hydraulic pumps and motors involves constant switching between high-pressure and low-pressure chambers, which can lead to pressure shocks that compromise motor performance and longevity. Researchers worldwide have diligently investigated methods to mitigate these pressure shocks. For example, Ref. [7] developed a design methodology using CASPAR to reduce pressure oscillation in piston pumps. Refs. [8, 9] implemented elastic rings within piston pumps to absorb pressure energy, effectively decreasing pressure pulsations. Additionally, Refs. [10, 11] employed finite element methods to model pump flow and piston chamber pressure, and a simplified cavitation model is introduced to analyze flow pulsations. Ref. [12] proposed a new valve plate structure to address noise issues caused by abrupt pressure changes in double shaft piston pumps. Ref. [13] designed a valve plate for electro-hydraulic servo swashplate plunger transformers. Refs. [14, 15] conducted simulation and experimental analyses on pressure impacts. Additionally, Refs. [16, 17] explored various buffer device designs, including triangular grooves and U-shaped grooves, to mitigate pressure shocks during the

① Supported by the National Natural Science Foundation of China (No. 52375037), the Masters Innovation Project of Beijing University of Civil Engineering and Architecture (No. PG2024142), the Outstanding Youth of Pyramid Talent Training Project of Beijing University of Civil Engineering and Architecture (No. GDRC20220801) and the Breeding Program Funding of Beijing University of Civil Engineering and Architecture (No. X24026).

② To whom correspondence should be addressed. E-mail: hitwangxiaojing@163.com.

Received on Mar. 11, 2024

operation of rotary electro-hydraulic servo motors.

By analyzing the research status at home and abroad, it is rare to observe the implementation of a novel cushioning structure to investigate the impact of pressure shocks on electro-hydraulic servo motors that spin continuously. Therefore, the mathematical models of triangular groove and U-shaped groove are established firstly, and the optimal size of the two buffer slots is obtained by Matlab. Secondly, the pressure gradient model for the motor seal chamber is established under the combined pressure grooves and the optimal dimensions of the combined pressure grooves depth and depth angle are obtained through the bird flock optimization algorithm. Finally, a three-dimensional model of the motor's internal flow field is established for the triangular groove and combined pressure groove. Subsequently, the internal flow field model is numerically calculated using Fluent software. The study investigates the distribution of the pressure field within the motor seal chamber under the triangular and combined pressure grooves to investigate the effects of the latter on pressure reversal.

1 Establishment of mathematical model for sealing cavity of continuous rotary electro-hydraulic servo motor

1.1 Mathematical model of motor seal cavity with triangular groove and U-groove structure

Fig. 1(a) illustrates the construction of a continuously rotating electro-hydraulic servo motor of the vane type. The motor comprises a vane, a rotor, a mating casing, and a stator. The vanes are pushed by a pre-compressed spring to form a sealed chamber within the motor, pressing against the stator when idle. To reduce pressure shocks during oil distribution, hydraulic pump and motor housings typically feature triangular and U-shaped grooves (Fig. 1(b)), which are constructed based on the plane angle and depth angle. These groove designs are commonly employed on the valve plate (Fig. 1(c)).

Eqs. (1) and (2) express the calculated circulation area of the triangular and U-shaped grooves, based on their respective structural schematic diagrams.

$$A = \frac{1}{2} r^2 \theta^2 \tan\gamma_1 \cos\frac{\gamma_2}{2} \tan\gamma_2 \quad (1)$$

where, r represents the radius at the leading edge of the motor valve distribution window in millimeters; θ indicates the angle (°) at which the motor blades rotate in the groove; γ_1 represents the plane angle, and γ_2 represents the depth angle of the groove.

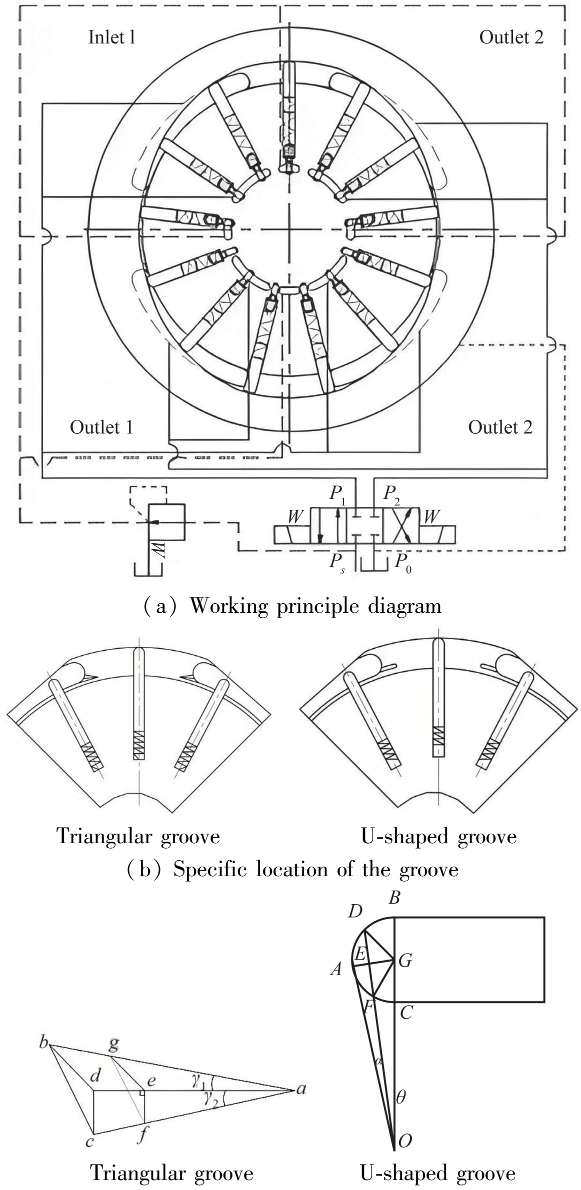

(a) Working principle diagram

(b) Specific location of the groove

(c) Theoretical analysis diagram of the groove

Fig. 1 Schematic diagram of the groove structure

The flow area of the U-groove expands swiftly upon entering the semi-cylindrical section and remains steady in the equivalent-sized area. The groove is divided into two sections: the semi-cylinder and the equal-area part. The angle of the semi-cylindrical section is denoted by α, with DF perpendicular to AG, $b = BC$, and $r = OC$.

$$A = \begin{cases} 2L\sqrt{\left(\frac{b}{2}\right)^2 - \left(\frac{b}{2} + r\right)^2 \sin^2(\theta - \alpha)} & \alpha < \theta \\ b \times L & \alpha \geqslant \theta \end{cases} \quad (2)$$

where, L is the depth of U-channel.

The capacity of the triangular buffer tanks and U-shaped tanks entering or exiting the motor sealing chamber will occur as in Eqs. (3) and (4).

$$\frac{\mathrm{d}V_1}{\mathrm{d}t} = \frac{1}{2}r^2\theta^2\tan\gamma_1\cos\frac{\gamma_2}{2}\tan\gamma_2 C_q\sqrt{\frac{2\Delta p}{\rho}} \tag{3}$$

$$\frac{\mathrm{d}V_2}{\mathrm{d}t} = \begin{cases} 2C_q L\sqrt{\left(\frac{b}{2}\right)^2 - \left(\frac{b}{2}+r\right)\sin^2(\theta-\alpha)}\sqrt{\frac{2\Delta p}{\rho}} & \alpha < \theta \\ bLC_q\sqrt{\frac{2\Delta p}{\rho}} & \alpha \geqslant \theta \end{cases} \tag{4}$$

where, Δp is the pressure difference between the inlet and the outlet.

The pressure gradient in the sealing cavity under the triangular buffer groove and U-shaped groove structure is calculated as in Eqs. (5) and (6).

$$\frac{\mathrm{d}p_1}{\mathrm{d}\theta} = -\frac{\beta_e}{\omega}\cdot\frac{\frac{1}{2}r^2\theta^2\tan\gamma_1\cos\frac{\gamma_2}{2}\tan\gamma_2 C_q\sqrt{\frac{2\Delta p}{\rho}}}{B\left[(R_1^2-R_2^2)\frac{\pi}{z}-(R_2-R_1)b\right]} \tag{5}$$

$$\frac{\mathrm{d}p_2}{\mathrm{d}\theta} = \begin{cases} -\frac{\beta_e}{\omega}\cdot\frac{2C_q L\sqrt{\left(\frac{b}{2}\right)^2-\left(\frac{b}{2}+r\right)\sin^2(\theta-\alpha)}\sqrt{\frac{2\Delta p}{\rho}}}{B\left[(R_1^2-R_2^2)\frac{\pi}{z}-(R_2-R_1)b\right]} \\ \alpha < \theta \\ -\frac{\beta_e}{\omega}\cdot\frac{bLC_q\sqrt{\frac{2\Delta p}{\rho}}}{B\left[(R_1^2-R_2^2)\frac{\pi}{z}-(R_2-R_1)b\right]} \\ \alpha \geqslant \theta \end{cases} \tag{6}$$

The relevant calculation parameters of numerical salution in this paper are listed in Table 1.

1.2 Simulation analysis

In the process of depressurizing the engine, the blade angle on the buffer slot is set to 3 °. Considering the dimensions of the injector plate in relation to the position of the buffer groove, and that the structure of the triangular groove can be considered as a triangular cone obtained by machining with a molding tool, the plane angle is set to $\gamma_1 = 8$ ° and the width angle is set to $\gamma_3 = 60$ °. For the triangular slot buffer optimization[18], the influence factor of the width angle is defined as $K_w = \tan(\gamma_3/2)$ and the influence factor of the depth angle is defined as $K_d = \tan\gamma_2\sin\gamma_2$, so the size of the depth angle ranges from 6.5 ° to 9.5 °. To study the influence of the triangular slot buffer tank structure on the pressure of the motor sealing tank, Matlab simulation is carried out, and the pressure change and pressure gradient change curves for different depth angles in the optimization interval under the triangular slot structure are obtained, as illustrated in Fig. 2.

Table 1 Parameters of numerical solution

Parameter	Physical meaning	Value
P_s	Oil source pressure	10.0 MPa
P_1	Inlet chamber pressure	6.5 MPa
P_2	Oil return chamber pressure	3.5 MPa
β_e	Bulk modulus of elasticity	700.0 MPa
z	Number of motor blades	13
ω	Motor speed	$0.1/(° \cdot s^{-1})$
R_2	Radius of the rotor	98.00 mm
R_1	Large arc radius of stator	112.50 mm
η	Dynamic viscosity coefficient	0.028 8 Pa · s
ρ	Oil density	$870\ kg \cdot m^{-3}$
C_q	Flow coefficient	0.82
B	Stator width	60.00 mm
r	Leading edge radius	98.00 mm
B_1	Gap width	14.50 mm
b	Blade thickness	8.00 mm
δ	Clearance height	0.01 mm

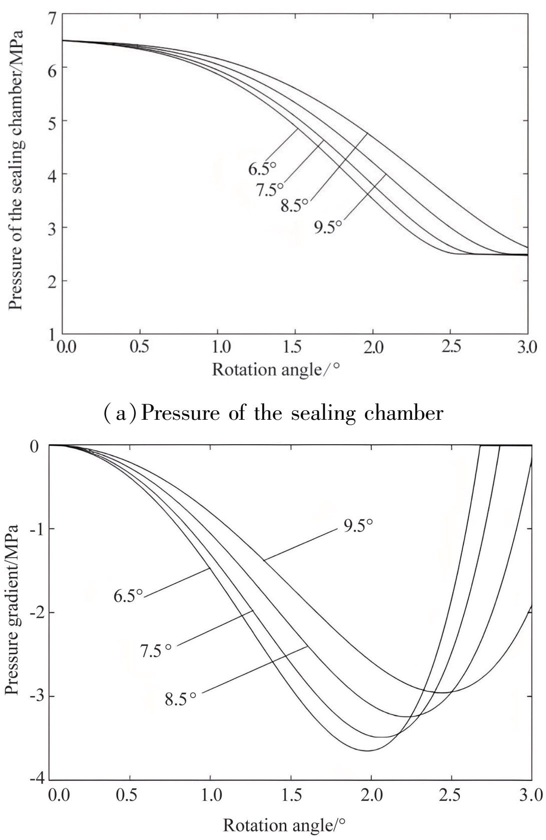

(a) Pressure of the sealing chamber

(b) Pressure gradient

Fig. 2 Pressure reduction curves of sealed cavity under triangular groove

Curves in Fig. 2 show pressure variations at depth angles of 6.5 °, 7.5 °, 8.5 °, and 9.5 ° respectively. In Fig. 2(a), the curve of 8.5 ° gradually decreases in pressure until it equals the output pressure. Fig. 2(b) indicates a significantly smaller pressure gradient change in the curve of 8.5 ° during decompression. Thus, maximum motor output power is achieved with a plane angle of 8.0 ° and a depth angle of 8.5 ° for the triangular cutout.

With the oil distribution board's dimensions and buffer tank placement in mind, the width of the U-shaped groove is set to 2.00 mm and the depth is taken to be like the depth of the largest cross section of the triangular groove, resulting in a depth range of 1.45 – 1.65 mm. Matlab is used to determine the optimum depth from 1.45 mm, 1.50 mm, 1.55 mm, and 1.65 mm, examining their impact on motor seal compartment pressure, as shown in Fig. 3.

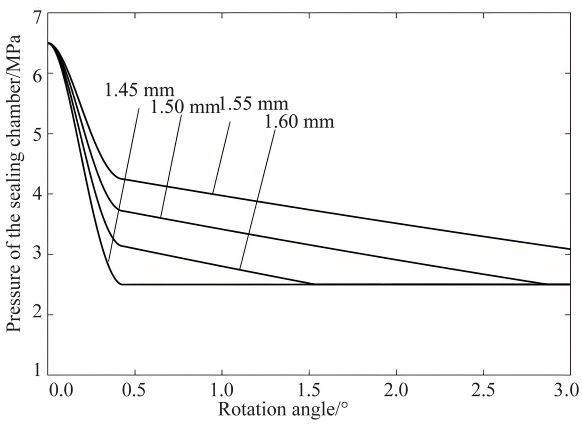

(a) Pressure of the sealing chambe

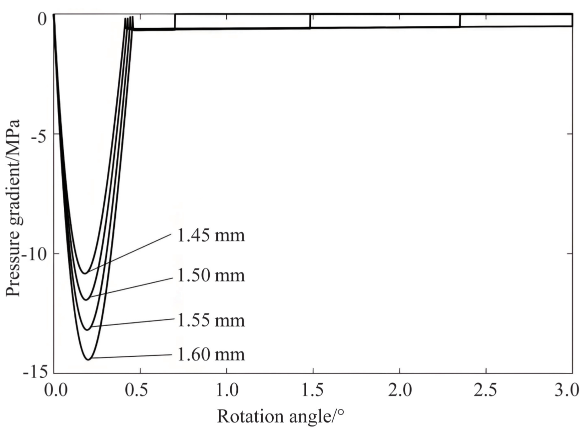

(b) Pressure gradient

Fig. 3 Pressure reduction curves of sealed volume under U-shaped groove

Fig. 3 depicts the depressurization curve under the U-shaped recess, with curves representing depths of 1.45 mm, 1.50 mm, 1.55 mm, and 1.65 mm respectively. The curve of 1.55 mm shows a gentle pressure drop and moderate gradient, aligning sealing chamber pressure with the outlet pressure. Additionally, the curve of 1.55 mm exhibits less significant changes in pressure gradient during depressurization. Optimal pressure reduction occurs with a U-groove width of 2.00 mm and a depth of 1.55 mm.

The triangular groove with plane angle 8 ° and depth angle 8.5 °, and U-shaped groove with width 2.00 mm and depth 1.55 mm are simulated and analyzed respectively. The simulation results are shown in Fig. 4.

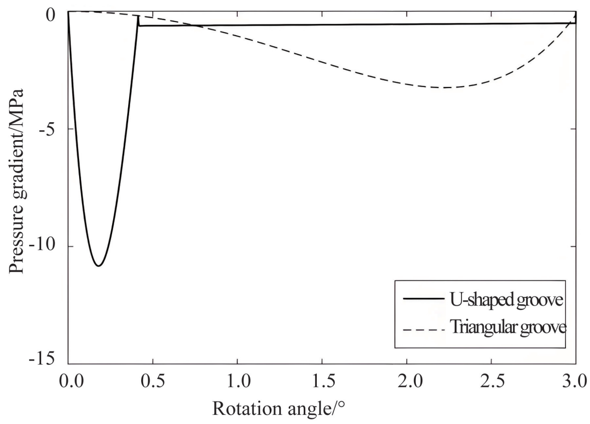

Fig. 4 The simulation results

Fig. 4 shows significant pressure gradient fluctuations with the U-shaped groove during depressurization, while the triangular groove exhibits minimal changes. Upon comparison, the triangular groove demonstrates superior pressure reduction capabilities.

2 Structure optimization of combined pressure buffer tank for continuous rotary electro-hydraulic servo motor

The bird flock optimization algorithm[19-22] facilitates the exchange of information between groups and achieves fast convergence by using group intelligence for effective problem solving, while effectively avoiding falling into local optimums. In this study, the pressure gradient model inside the motor sealing chamber in the presence of a combination of grooves is investigated, and the dimensioning of the combination of grooves is optimized based on the solution steps of the bird flock optimization algorithm. A groove structure is considered in the study, in which the vanes pass through the triangular and U-shaped grooves sequentially. To maintain the sealing effect, the blades are rotated at an angle of 3 ° on the combined groove. Furthermore, it is crucial to ensure that the combined pressure groove area is commensurate with that of the two cushion grooves. The ratio of the triangular groove to the U-shaped groove area is 2 : 3[23-25]. By employing this ratio, the two phases of the blade turning angle can be calculated with precision. Furthermore, the throttle bore flow equation assists in determining the quantity of hydraulic fluid entering and exiting the motor seal chamber through the combined pressure tank, thereby effectively eliminating any possibility of leakage from the motor. The expression for the flow area under the combined groove is as follows.

$$\frac{\mathrm{d}V}{\mathrm{d}t} = \begin{cases} \frac{1}{2}C_q r^2\theta^2 \tan\gamma_1 \cos\frac{\gamma_2}{2}\tan\gamma_2\sqrt{\frac{2\Delta p}{\rho}} & 0.0° \leqslant \theta < 1.2° \\ C_q\, 2L\sqrt{\left(\frac{b}{2}\right)^2 - \left(\frac{b}{2}+r\right)\sin^2(\theta - 0.57)}\sqrt{\frac{2\Delta p}{\rho}} & 1.2° \leqslant \theta < 1.77° \\ C_q bL\sqrt{\frac{2\Delta p}{\rho}} & 1.77° \leqslant \theta < 3.0° \end{cases} \quad (7)$$

where, θ represents the angle at which the blade rotates through the pressure groove combination.

The pressure gradient equation of the sealing cavity of the motor under the combined groove structure is as follows.

$$\frac{\mathrm{d}p}{\mathrm{d}\theta} = \begin{cases} -\frac{\beta_e}{\omega}\cdot\frac{\frac{1}{2}C_q r^2\theta^2\tan\gamma_1\cos\frac{\gamma_2}{2}\tan\gamma_2\sqrt{\frac{2\Delta p}{\rho}}}{B\left[(R_1^2 - R_2^2)\frac{\pi}{13} - (R_2 - R_1)b\right]} & 0.0° \leqslant \theta < 1.2° \\ -\frac{\beta_e}{\omega}\cdot\frac{2LC_q\sqrt{\left(\frac{b}{2}\right)^2 - \left(\frac{b}{2}+r\right)\sin^2(\theta-0.57)}\sqrt{\frac{2\Delta p}{\rho}}}{B\left[(R_1^2 - R_2^2)\frac{\pi}{13} - (R_2 - R_1)b\right]} & 1.2° \leqslant \theta < 1.77° \\ -\frac{\beta_e}{\omega}\cdot\frac{C_q bL\sqrt{\frac{2\Delta p}{\rho}}}{B\left[(R_1^2 - R_2^2)\frac{\pi}{13} - (R_2 - R_1)b\right]} & 1.77° \leqslant \theta < 3.0° \end{cases} \quad (8)$$

The position of the bird flock is determined by the depth and angle dimensions of the combined pressure groove, represented as C_{i1} and C_{i2}. During decompression, the pressure gradient equation of the motor is implemented as the objective function for the purpose of computing the flock adaptation values, denoted as $F(x)$.

$$F(x) = \begin{cases} -\frac{\beta_e}{\omega}\cdot\frac{\frac{1}{2}C_q r^2\theta^2\tan\gamma_1\cos\frac{C_{i2}}{2}\tan C_{i\,2}\sqrt{\frac{2\Delta p}{\rho}}}{B\left[(R_1^2 - R_2^2)\frac{\pi}{13} - (R_2 - R_1)b\right]} & 0.0° \leqslant \theta < 1.2° \\ -\frac{\beta_e}{\omega}\cdot\frac{2C_{i1}C_q\sqrt{\left(\frac{b}{2}\right)^2 - \left(\frac{b}{2}+r\right)\sin^2(\theta-0.57)}\sqrt{\frac{2\Delta p}{\rho}}}{B\left[(R_1^2 - R_2^2)\frac{\pi}{13} - (R_2 - R_1)b\right]} & 1.2° \leqslant \theta < 1.77° \\ -\frac{\beta_e}{\omega}\cdot\frac{C_q bC_{i1}\sqrt{\frac{2\Delta p}{\rho}}}{B\left[(R_1^2 - R_2^2)\frac{\pi}{13} - (R_2 - R_1)b\right]} & 1.77° \leqslant \theta < 3.0° \end{cases} \quad (9)$$

In the continuous rotary electro-hydraulic servo motor bucking process, the motor blades must be limited to a maximum rotation of 3.0° on the combined pressure tank to form a sealing cavity, that is, when the blaed is rotated from 0.0° to 3.0°, the pressure reduction can be completed, so the motor blade rotation angle constraints are shown below.

$0.0° < \theta < 3.0°$

In the combined groove, the U-shaped groove depth dimension interval is constrained as follows.

$1.45\ \text{mm} < L < 1.65\ \text{mm}$

The dimension interval of the depth angle of the triangular groove in the combined groove is constrained as follows.

$6.5^{\circ} < \gamma_2 < 9.5^{\circ}$

The decision function, based on the motor's pressure gradient during depressurization, optimizes combined pressure groove parameters constrained by the rotation angle of the motor blade and groove size. Ten birds, one spatial dimension, and 600 iterations are used. Flight frequency is 8, with cognitive and social evolution coefficients set to 1, and parameters a_1 and a_2 are also 1. Matlab simulates the objective function, shown in Fig. 5.

To minimize the pressure gradient of the motor during depressurization, the fitness function is tested with various values. The optimization curve of the objective function (Fig. 5 (a)) shows convergence to −1.274 1 at the 53rd iteration. Fig. 5(b) reveals that the pressure gradient is minimized when the depth angle is 9.41 ° and the depth is 1.532 mm. Therefore, the maximum pressure reduction is achieved for a combined pressure groove with a 2.000 mm width, 8.00 ° plane angle, 9.41 ° depth angle, and 1.532 mm depth.

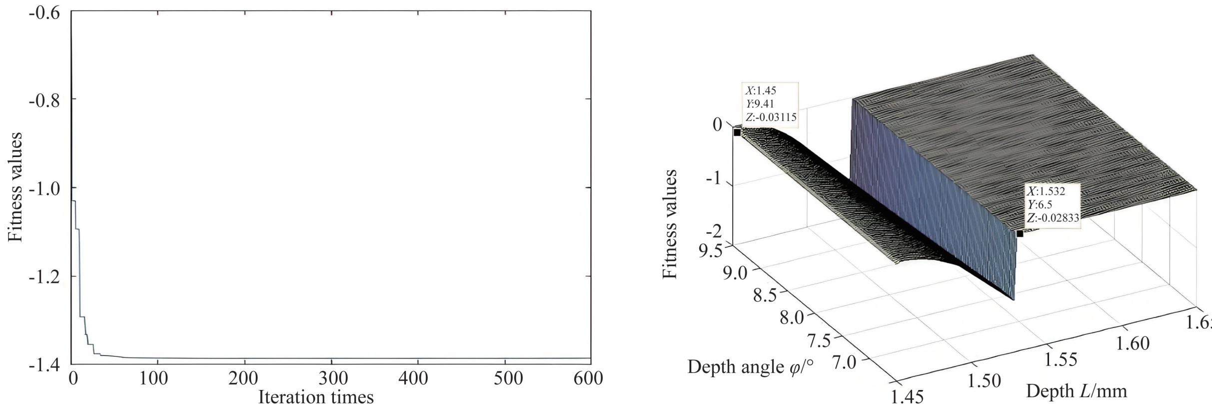

(a) Optimization curve of objective function (b) Optimized curve of depth and depth angle of combined slot

Fig. 5 The optimization result of bird swarm algorithm

3 Simulation and analysis of internal flow field of continuous rotary electro-hydraulic servo motor

3.1 Before processing

To assess the impact of triangular and combined slot structures on pressure in the long radius arc region of the motor, the vanes are rotated by 0.4 ° from their tangent position to the oil return chamber. The internal flow field in the motor seal cavity was modelled using unigraphics NX (UG) software with adjacent vanes rotating from 0.0 ° to 3.2 °. In the model of the motor's internal flow field, accurate numerical calculations require a refined mesh due to the smaller gap between the top of the motor blade and the contacting part of the stator surface and the smaller size of the part at the sharp corner of the triangular slot. The internal flow field mesh model in the decompression process with delta slot and combined slot structure in the long radius region after refinement is shown in Fig. 6(a) and (b). Fig. 6(c) and (d) display the improved mesh model of the internal flow field during pressurization in the short radius region using a triangular slot and combined slot structure.

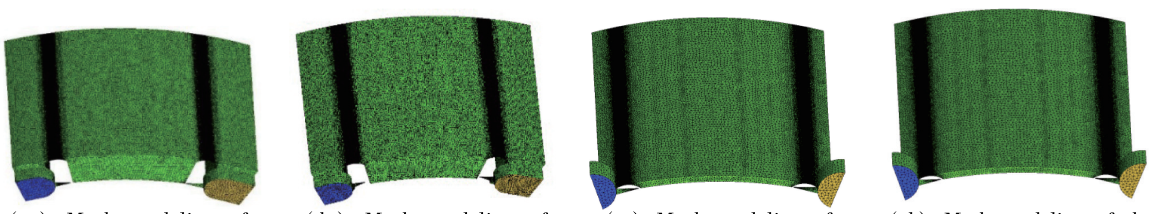

(a) Mesh modeling of the flow field in the Madanai under the triangular slot structure of the buckling process (b) Mesh modeling of the flow field in the Madanai under the combined slot structure of the buckling process (c) Mesh modeling of the flow field in the Madanai under the triangular slot structure of the boosting process (d) Mesh modeling of the flow field in the Madanai under the combined pressure tank structure of the boosting process

Fig. 6 Internal flow field grid model of the motor

The mesh model is calculated in Fluent, and the material property is set as No. 32 anti-wear hydraulic oil. The boundary conditions are defined as 6.5 MPa and 3.5 MPa at the pressure inlet and outlet. A renormalization group (RNG) turbulence model is selected as the solver.

3.2 Flow field simulation of motor seal cavity

The pressure changes in the motor sealing chamber at different rotation angles of the blades under the triangular slot structure and the combined slot structure were derived from the results of the 3D model of the internal flow field of the motor, processed using the computational fluid dynamics-post processing (CFD-POST) software. The motor blade rotation angle of 0.4 ° is the rotation interval, and the checked rotation angles are 0.0°, 0.4 °, 0.8 °, 1.2 °, 1.6 °, 2.0 °, 2.4 °, 2.8 °, and 3.2 °, as shown in Figs. 7 and 8.

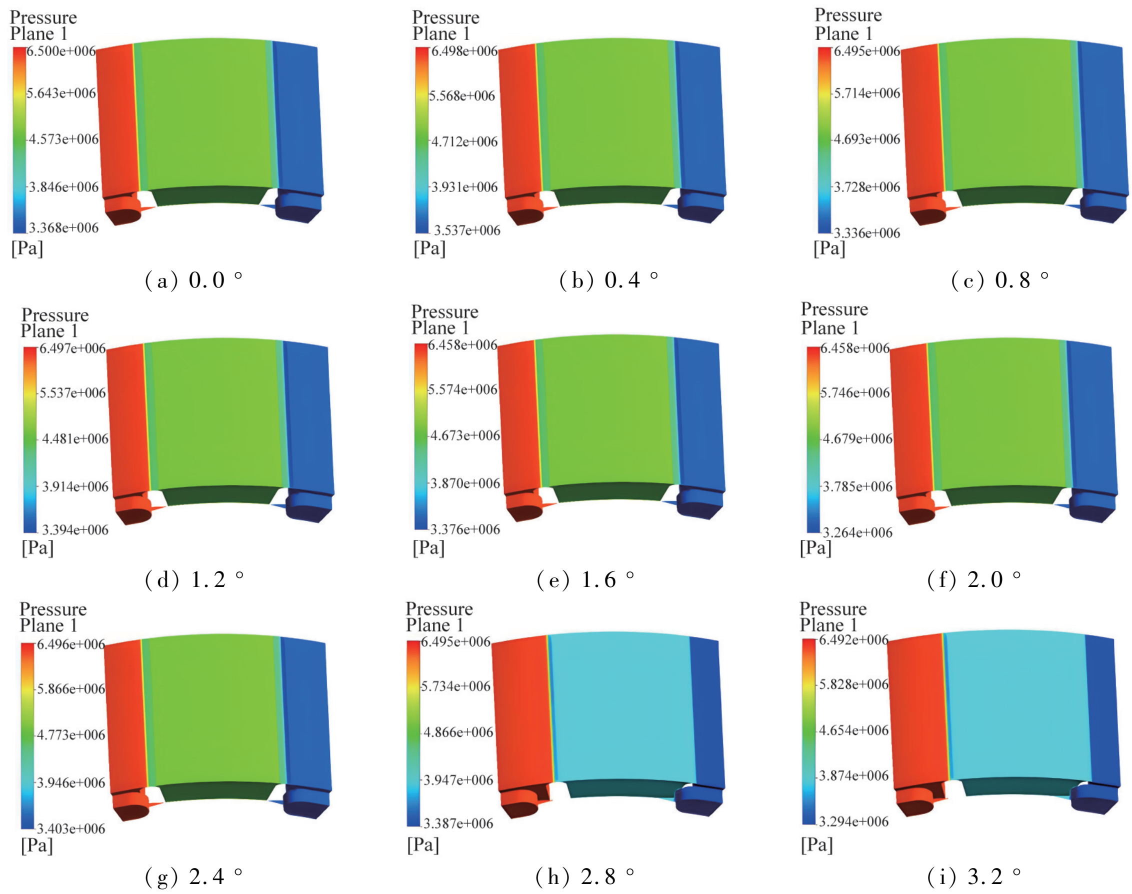

Fig. 7 Calculation results of the motor seal cavity under the triangular groove

As can be observed from the flow and pressure diagrams in the motor, the pressure within the engine seal chamber varies constantly and demonstrates a downward trend as the motor blades rotate. During the depressurization process, the pressure fluctuates but it is not consistently stable. When the motor blade rotation angle reaches 3.2 °, the sealing chamber of the motor is linked to the oil return chamber, finishing the pressure reduction in the sealing chamber.

To analyze the effect of two buffer groove types on motor pressure during depressurization in the long radius arc area, pressure values are recorded under both groove types at various blade rotation angles. Matlab is then used to plot pressure change and pressure gradient curves in the motor seal chamber, as shown in Fig. 9 (a) and (b).

Fig. 9(a) illustrates the occurrence of significant pressure fluctuations during the depressurization process in the region of the long radius arc, situated below the triangular notch. In contrast, the combined notch structure effectively mitigates these fluctuations, thereby ensuring a more stable decompression process. As illustrated in Fig. 9(b), the combined groove has been observed to significantly reduce the range of pressure gradients within the seal cavity in comparison to a single triangular groove. In conclusion, the combined groove structure has been demonstrated to be more effective in mitigating pressure shocks during the pressure reduction process.

The calculated pressure changes in the motor seal chamber during pressurization reflect the pressure fluctuations in the motor blades, which are affected by the triangular and combined slot configurations at different rotation angles (from 0.0 ° to 3.2 °). As the rotation angle of the motor blades increases, the pressure inside the seal chamber demonstrates an overall increasing trend, particularly at 3.2 ° of rotation, with a significant surge in pressure, which is particularly evident in the pressure distribution plots.

Pressure and pressure gradient curves within the motor seal chamber during the boosting process under the triangular slot and combined slot structures are presented in Fig. 10(a) and (b), respectively.

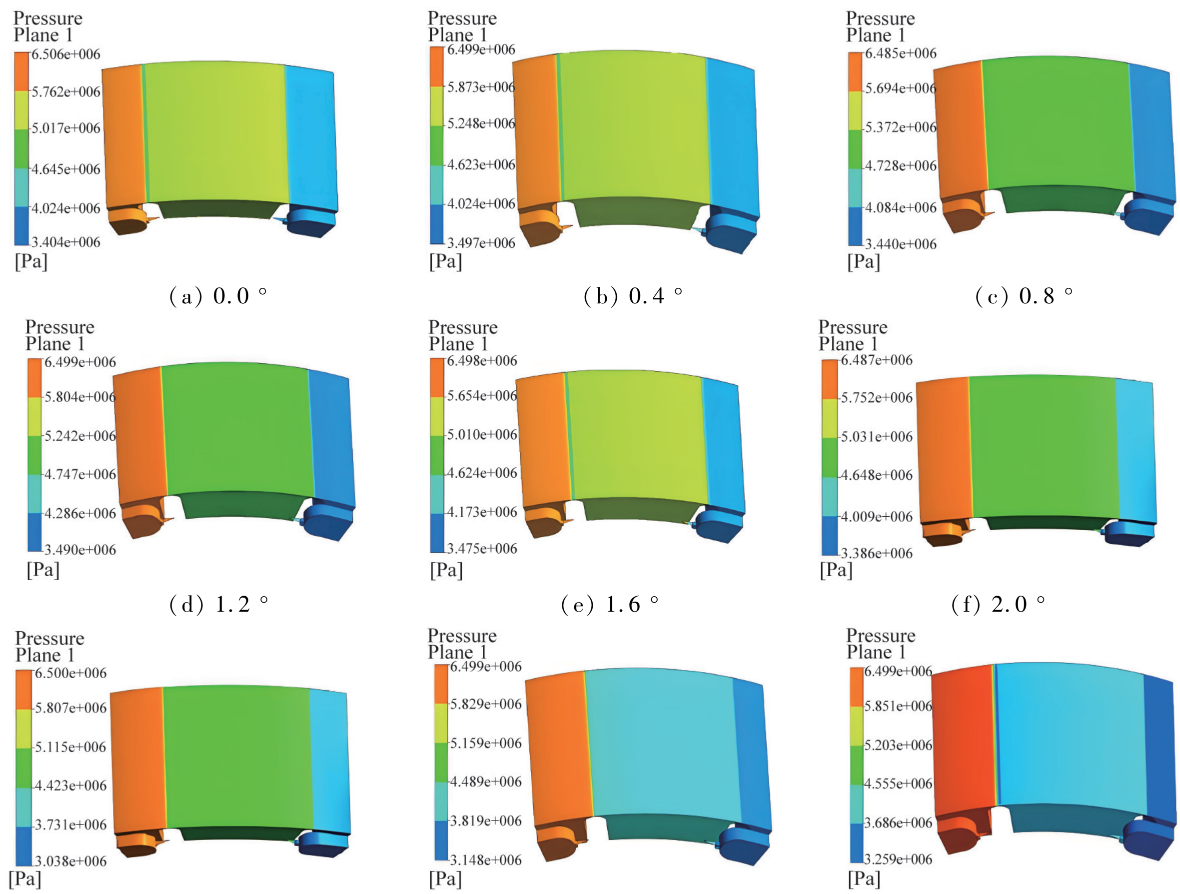

(a) 0.0 ° (b) 0.4 ° (c) 0.8 °
(d) 1.2 ° (e) 1.6 ° (f) 2.0 °
(g) 2.4 ° (h) 2.8 ° (i) 3.2 °

Fig. 8 Calculation results of the motor seal cavity under the combined groove

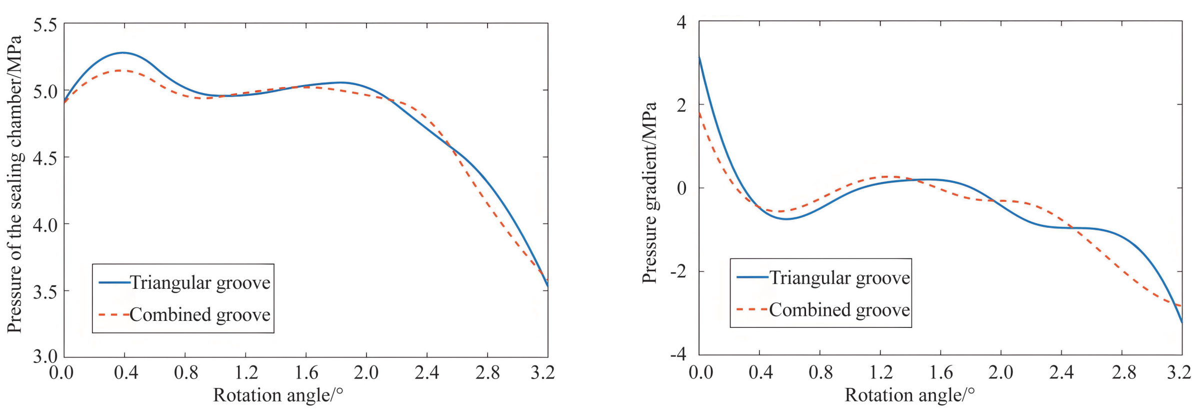

(a) Pressure of the sealing chamber (b) Pressure gradient

Fig. 9 Decompression curves of motor seal cavity

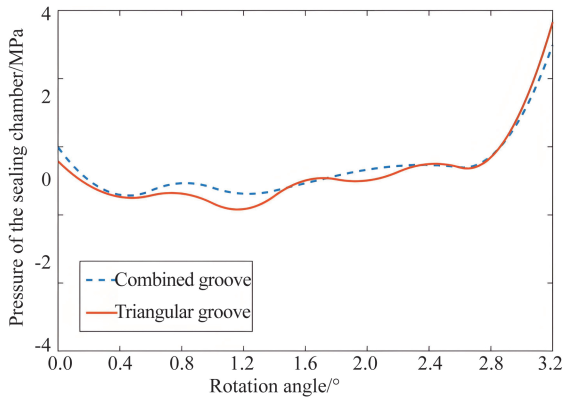

(a) Pressure of the sealing chamber

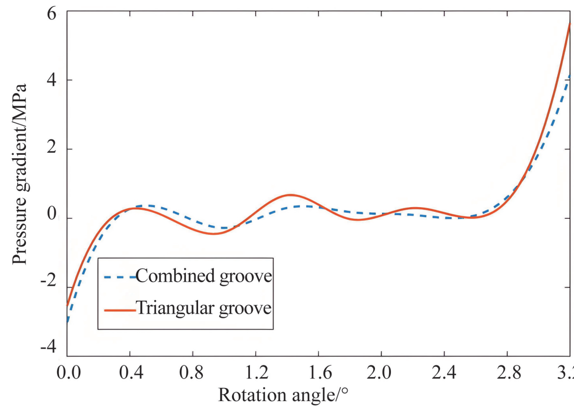

(b) Pressure gradient

Fig. 10 Boosting curve of motor seal cavity

The analysis on Fig. 10(a) shows significant pressure fluctuations in the sealing cavity under the triangular groove structure during supercharging, whereas the fluctuations are milder under the combined pressure tank structure, ensuring a more stable process. In Fig. 10(b), the pressure gradient in the sealing cavity is significantly lower under the combined pressure groove structure during supercharging compared with the triangular groove. Overall, the combined pressure grooves prove to be more effective in mitigating the pressure surges experienced by the engine during supercharging.

4 Conclusions

(1) By analyzing the working principle of continuous rotary electro-hydraulic servo motor, the sealing cavity model of the motor with triangular groove, U-groove and combined pressure groove is established. By analyzing pressure and pressure gradient curves in the motor workshop with varying buffer groove structures, it can be concluded that the most effective pressure reduction during the depressurization process is achieved with the triangular groove angle at 8.0 ° and the depth angle at 8.5 °. The most optimal pressure reduction results are accomplished with a U-groove width of 2.00 mm and a depth of 1.55 mm. When the combined pressure groove width is 2.00 mm, the plane angle is 8.00 °, the depth angle is 9.41 °, and the depth is 1.532 mm, the depression-reducing effect reaches its optimum level.

(2) By analyzing the pressure and pressure gradient curves at the optimal dimensions for both triangular and U-shaped grooves, it can be concluded that the decompression effect of the triangular groove is more significant than that of the U-groove.

(3) From the pressure cloud diagram, pressure curves and pressure gradient curves under triangular and combination grooves during the depressurization and boosting processes, it can be concluded that the combined groove structure can effectively relieve the pressure shock when the high- and low-pressure chambers of the motor are reversed.

References

[1] YAN W P. Research on key seal and component of swing electro-hydraulic servo motor applied to simulator [D]. Harbin: Harbin Institute of Technology, 2013. (In Chinese)
[2] LI Z. Research on control methods of high precision turntable [D]. Xi'an: Xidian University, 2014. (In Chinese)
[3] GUO J J, MA S J, ZHANG X J Z, et al. Research on CNC machining technology of the upper shell of electro-hydraulic servo valve [C]//Journal of Physics: Conference Series. Bristol, UK: IOP Publishing, 2020: 1-8.
[4] LI T Y, CHEN T T, YE K, et al. Research and simulation of marine electro-hydraulic steering gear system based on EASY5 [C]//2019 IEEE 3rd Information Technology, Networking, Electronic and Automation Control Conference. Chengdu, China: IEEE, 2019: 1972-1979.
[5] WANG B Y, WNAG Y P, LIANG Y, et al. Design on articular motion & servo driving with experimental analysis for lower limb exoskeleton robot [J]. Chinese Journal of Mechanical Engineering, 2019, 55(23): 55-66. (In Chinese)
[6] PUGI L, ALFATTI F, BERZI L, et al. Fast modelling and identification of hydraulic brake plants for automotive applications [J]. International Journal of Fluid Power, 2020, 21 (2): 169-210.
[7] JONATHAN E B, IVANTYSYNOVA M. Power loss in the lubricating gap between cylinder block and valve plate of swash plate type axial piston machines [J]. International Journal of Fluid Power, 2009, 10(2): 29-43.
[8] BECHER D, HELDUSER S. Innovation pump design to reduce pressure pulsations of axial piston pumps [J]. Workshop on Power Transmission and Motion Control, 2000, 23(4): 232-234.

[9] BECHER D. Untersuchungen an einer axialkolbenpumpe mit ringsystem zur mingerung vonpulsationen [D]. Dresden: TU Dresden, 2004. (In German)
[10] CASOLI P, VACCA A. Modeling of an axial piston pump for pressure ripple analysis[C]// The 8th Scandinavian International Conference on Fluid Power. Tampere, Finland: SICFP, 2003: 469-472.
[11] CASOLI P, VACCA A, FRANZONI G, et al. Modelling of fluid properties in hydraulic positive displacement machines [J]. Simulation Modelling Practice and Theory, 2006, 14(8): 1059-1072.
[12] PAN Y, LI Y B, HUANG M H, et al. Valve plate improvement and flow ripple characteristic analysis for double compound axial piston pump [J]. Transactions of the Chinese Society for Agricultural Machinery, 2016, 47(4): 391-398.
[13] LIU C Q, JIANG J H, GAO L X, et al. Valve plate's buffer slot in electro-hydraulic servo plate-inclined plunger hydraulic transformer [J]. Journal of Harbin Institute of Technology, 2013, 45(7): 53-56.
[14] XU B, SONG Y C, YANG H Y. Pre-compression volume on flow ripple reduction of a piston pump [J]. Chinese Journal of Mechanical Engineering, 2013, 26(6): 1259-1266.
[15] XU B, YE S G, ZHANG J H, et al. Flow ripple reduction of an axial piston pump by a combination of cross-angle and pressure relief grooves: analysis and optimization [J]. Journal of Mechanical Science and Technology, 2016, 30(6): 2531-2545.
[16] WANG X J, HU T L, SHEN Z Q. Pressure impact characteristic of vane type continuous rotary motor under different buffer structures [J]. Journal of Central South University: English Edition, 2020, 27(12): 3652-3666.
[17] WANG Y X. Study on damping groove characteristics and optimization of axial piston pump [D]. Zhejiang: Zhejiang University, 2014. (In Chinese)
[18] WANG C Y. Research on the effect of unloading groove on the output pressure and cavitation characteristics of axial piston pumps [D]. Changsha: Central South University, 2023. (In Chinese)
[19] MENG X B, GAO X Z, LU L, et al. A new bio-inspired optimization algorithm: bird swarm algorithm [J]. Journal of Experimental and Theoretical Artificial Intelligence, 2016, 28(4): 1-15.
[20] TAO Y. Fault diagnosis of ship relay protection system based on bird swarm fly algorithm [D]. Zhenjiang: Jiangsu University of Science and Technology, 2019. (In Chinese)
[21] LI C Y, PEI L G, ZHANG X, et al. A method of setting transmission and distribution price by voltage level based on bird swarm algorithm [J]. Power System and Clean Energy, 2019, 35(4):37-42. (In Chinese)
[22] WANG X, YANG X Y, FAN X Q, et. al. Application of flow analysis and bird flock optimization in Feng Shui cooperative operation [J]. Power Generation Technology, 2018, 39(2): 171-176.
[23] XIE S C. Optimization and analysis of damping groove structure of valve plate of axial piston pump based on pumplinx [D]. Lanzhou: Lanzhou University of Technology, 2019. (In Chinese)
[24] ZHANG J, XIE S C, YANG F L, et al. The optimization of axis pump valve plate triangular groove structure based on PumpLinx [J]. Hydropneumatics and Sealing, 2019, 39(12):14-19. (In Chinese)
[25] SONG Y N, SONG Y J, XU X C. Study on flow field optimization of flow distribution disk of double-unloaded groove piston pump [J]. Machine Tool and Hydraulics, 2020, 48(3): 159-163.

WANG Xiaojing, born in 1981. She received her Ph. D degree from Harbin Institute of Technology in 2009. Her main research interests are fluid transmission and control, new hydraulic components and devices, electro-hydraulic servo control system, digital hydraulic components, intelligent building hydraulic system, etc.